

Anion-driven mesogenicity: a comparative study of ionic liquid crystals based on the $[closo-1-CB_9H_{10}]^-$ and $[closo-1-CB_{11}H_{12}]^-$ clusters†

Bryan Ringstrand,^a Aleksandra Jankowiak,^a Lillian E. Johnson,^a Piotr Kaszynski,^{*ab} Damian Pocięcha^c and Ewa Górecka^c

Received 25th October 2011, Accepted 16th January 2012

DOI: 10.1039/c2jm15448j

A series of structurally analogous esters derived from monocarbaborates, $[closo-1-CB_9H_{10}]^-$ (**A**) and $[closo-1-CB_{11}H_{12}]^-$ (**B**), containing a maximum of 4 rings in the rigid core were prepared and investigated by thermal, optical, and XRD methods. Ion pairs containing a total of 4 rings with either *N*-butyl-4-heptyloxy pyridinium (**Pyr**) or cetyltrimethylammonium (**Cetyl**) cation form a SmA phase ranging from 90 °C to 229 °C. Ion pairs **1e[Pyr]** and **2e[Pyr]** containing an azo group in the anisometric anion exhibit an enantiotropic nematic phase above the SmA phase. The cesium salt **1h[Cs]** did not exhibit mesogenic behavior. Partial binary phase diagrams were investigated for **1d[Pyr]** and **2d[Pyr]** in **2e[Pyr]**, and for **1f[Pyr]** in non-ionic mesogens. Variable temperature powder XRD analysis of 5 ionic liquid crystals, **1e[Pyr]**, **1f[Pyr]**, **2f[Pyr]**, **1g[Pyr]**, and **2g[Pyr]**, demonstrated about 20% interdigitation in the SmA phase and provided thermal expansion coefficients.

Introduction

During the past decade, research on ionic liquid crystals (ILCs) has significantly intensified and diversified.^{1,2} One of the key attributes of this class of materials is anisotropic ion mobility, which is of considerable interest for developing ion-conductive materials³⁻⁷ for applications in batteries⁸ and dye-sensitized solar cells.⁹ The majority of ILCs investigated to date are derived from an anisometric cation, such as substituted ammonium, imidazolium, or pyridinium. The anion in these materials is present for charge compensation, although it can significantly affect mesophase range and stability.²

closo-Monocarbaborates $[closo-1-CB_9H_{10}]^-$ and $[closo-1-CB_{11}H_{12}]^-$ (**A** and **B**, respectively, Fig. 1), are symmetrical and weakly coordinating anions,¹⁰ and therefore are attractive structural elements for anion-driven ILCs. In this context, we recently reported the first examples of such derivatives (**IA**) containing the $[closo-1-CB_9H_{10}]^-$ cluster (**A**).¹¹ These ILCs, including esters **1a–1c**, display SmA and soft crystalline phases, when 3 rings are present in the rigid core and the charge is compensated with an elongated pyridinium cation, **Pyr**.

We are interested in the more accessible $[closo-1-CB_{11}H_{12}]^-$ cluster (**B**) as a structural element of ILCs (**IB**) capable of

supporting anisotropic lithium ion transport. To this end, we report the preparation and properties of a series of ILC esters **2** derived from cluster **B**. We investigate ion pairs of the anisometric anion containing a maximum of 4 rigid elements (3 rings and the monocarbaborate cage) in the rigid core with two different cations Q^+ , pyridinium (**Pyr**) and cetyltrimethylammonium (**Cetyl**, Fig. 2), and demonstrate the preparation of one ion pair with the Cs^+ cation. We compare their properties to analogous esters **1** derived from the $[closo-1-CB_9H_{10}]^-$ cluster (**A**) and study several binary mixtures. Finally, we establish fundamental structure-property relationships between the two series of ion pairs **1** and **2** using polarizing optical microscopy (POM), differential scanning calorimetry (DSC), and X-ray powder diffraction (XRD).

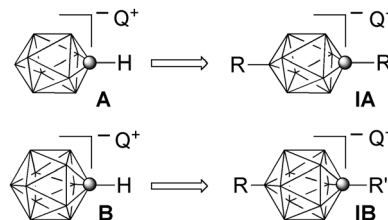


Fig. 1 The structures of the $[closo-1-CB_9H_{10}]^-$ and $[closo-1-CB_{11}H_{12}]^-$ clusters (**A** and **B**), and ion pairs of their 1,10- (**IA**) and 1,12-disubstituted (**IB**) derivatives with the counterion Q^+ . Q^+ represents a metal or an onium ion such as ammonium or pyridinium. Each vertex represents a BH fragment and the sphere is a carbon atom.

^aOrganic Materials Research Group, Department of Chemistry, Vanderbilt University, Nashville, TN 37235, USA

^bFaculty of Chemistry, University of Łódź, 91403 Łódź, Poland

^cDepartment of Chemistry, Warsaw University, 02-089 Warsaw, Poland

† Electronic Supplementary Information (ESI) available: synthesis details and analytical data for mesogens and their intermediates, additional powder XRD data, and molecular modeling details. See DOI: 10.1039/c2jm15448j

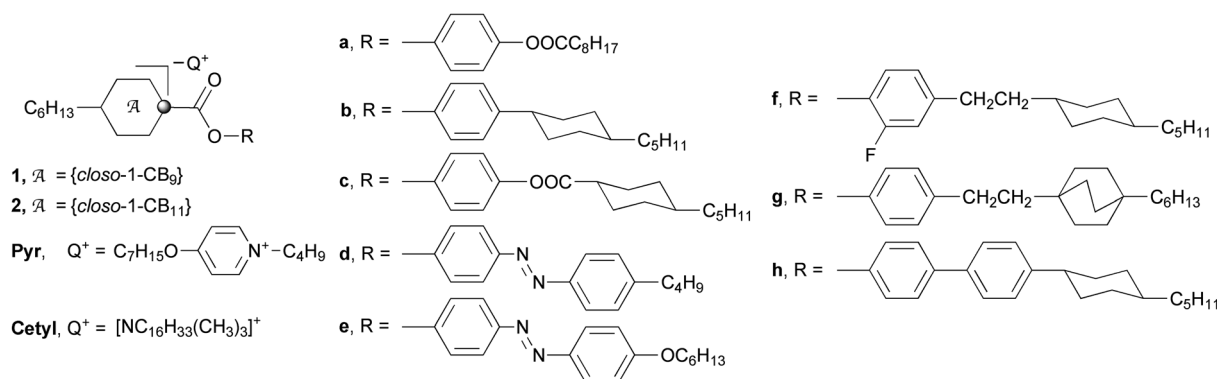


Fig. 2 Structures of series 1 and 2. For the definition of ring A see Fig. 1.

Results and discussion

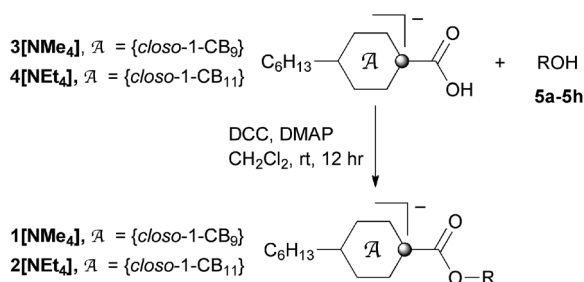
Synthesis

Esters **1**[NMe₄] and **2**[NEt₄] were prepared from carboxylic acids, **3**[NMe₄] and **4**[NEt₄], respectively, and phenols **5a–5h** using dicyclohexylcarbodiimide (DCC) and catalytic amounts of 4-dimethylaminopyridine (DMAP) in CH₂Cl₂ following a general literature procedure¹² (Scheme 1).

Esters **1**[Pyr] and **2**[Pyr] or **1**[Cetyl] and **2**[Cetyl] were prepared by exchange of the [NMe₄]⁺ or [NEt₄]⁺ cation for *N*-butyl-4-heptyloxy pyridinium (Pyr) or cetyltrimethylammonium (Cetyl) in a biphasic CH₂Cl₂/H₂O system following the procedure reported for the preparation of esters **1a**[Pyr]-**1c**[Pyr].¹¹ The Cs⁺ containing ion pair, **1h**[Cs], was prepared first by converting **1h**[NMe₄] to its acid form **1h**[H₃O], followed by treatment with CsCl and extraction of the **1h**[Cs] ion pair to CH₂Cl₂. The product was crystallized from toluene containing a few drops of MeCN to give the salt as a solvate with MeCN.

The carboxylic acid [closo-1-CB₁₁H₁₀-1-COOH-12-C₆H₁₃]⁻[NEt₄]⁺ (**4**[NEt₄]) was prepared from iodo acid [closo-1-CB₁₁H₁₀-1-COOH-12-I]⁻[NEt₄]⁺ (**6**[NEt₄]) using the Negishi coupling^{13,14} with excess hexylzinc chloride, as was previously described for the preparation of [closo-1-CB₉H₈-1-COOH-10-C₆H₁₃]⁻[NMe₄]⁺ (**3**[NMe₄]) (Scheme 2).¹¹ The PCy₃ ligand generated *in situ* works equally well for both acids, and the 12-hexyl acid **4**[NEt₄] was obtained in 61% yield.

Iodo acid **6**[NEt₄] was prepared in about 70% yield by lithiation of iodo derivative [closo-1-CB₁₁H₁₁-12-I]⁻ (either as Cs⁺ salt **7**[Cs] or as a trimethylammonium salt **7**[NHMe₃]) with *n*-BuLi in the presence of TMEDA, followed by reaction with CO₂



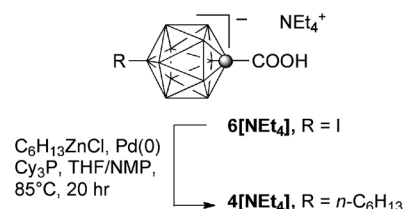
Scheme 1 Synthesis of esters **1**[NMe₄] and **2**[NEt₄]

(Scheme 3). Without TMEDA, the carboxylation of **7** was incomplete and only 20% conversion to **6** was observed. The iodo derivative **7** was prepared in 75% yield by iodination of the parent anion [closo-1-CB₁₁H₁₂]⁻ with I₂ in acetic acid.¹⁵ Alternatively, the carboxylic acid **6** (as **6**[NHMe₃]) can be obtained by carboxylation of **B** followed by iodination, according to a recent report.¹⁶ Considering that the parent anion **B** can be obtained in 2 steps and 65% yield from B₁₀H₁₄,¹⁷ the preparation of acid **4**[NEt₄] is a 5-step process with an overall yield of about 20%. In comparison with the 10-vertex analogue, acid **3**[NMe₄], the preparation of **4**[NEt₄] requires 1 fewer step, no isomer separation, and is nearly 5 times more efficient.^{11,18}

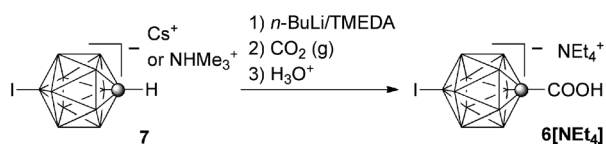
Liquid crystalline properties

Transition temperatures and associated enthalpies for compounds **1**[Pyr] and **2**[Pyr] and for **1**[Cetyl] and **2**[Cetyl] are shown in Tables 1 and 2, respectively. Phase structures were assigned by comparison of POM results with published textures for reference compounds¹⁹ and using powder XRD data. Ion pairs containing the [NMe₄]⁺ or [NEt₄]⁺ cations were not investigated for liquid crystalline properties based on previous results, which showed that these types of cations do not support the liquid crystalline state.¹¹ The cesium salt **1h**[Cs] did not melt below 300 °C.

Pyridinium salts containing a total of two rings (including the monocarbaborate cage) in the rigid core, **1a**[Pyr] and **2a**[Pyr], do not form liquid crystalline phases, while most pyridinium salts of three-ring anions form SmA phases (Table 1). The azo esters **1d**[Pyr] and **2d**[Pyr] with the butyl substituent are not liquid crystalline. However, inserting an OCH₂CH₂ group between the butyl chain and the phenyl ring induces a SmA phase: enantiotropic in **1e**[Pyr] (Fig. 3) and monotropic in **2e**[Pyr]. In addition, both hexyloxy derivatives exhibit a narrow enantiotropic



Scheme 2 Preparation of carboxylic acid **4**[NEt₄].



Scheme 3 Preparation of carboxylic acid **6[NEt₄]**.

nematic phase with the characteristic schlieren texture (Fig. 4a) above the fan texture of SmA (Fig. 4b). This is an interesting finding, since nematic phases are rare among ILCs and found only in some onium²⁰ and metallomesogenic²¹ ILCs. A comparison of N–I virtual transition temperatures, $[T_{N-I}]$, for the butyl derivatives **1d[Pyr]** and **2d[Pyr]** (*vide infra*) with those for the hexyloxy analogues demonstrated that the insertion of the OCH₂CH₂ group increases stability of the nematic phase by 27 K and 22 K respectively. For comparison, the same insertion of the OCH₂CH₂ group in non-ionic azobenzene derivatives increases the N–I transition temperature by about 45 K.^{22,23}

The cyclohexylphenyl derivative of {*closo*-1-CB₉}, **1b[Pyr]**, exhibits a narrow SmA phase (10 K) and two soft crystalline

phases.¹¹ Replacement of the 10-vertex cage with {*closo*-1-CB₁₁} in **2b[Pyr]** increases the melting point by 50 K and eliminates all mesogenic behavior. The observed higher melting temperature for **2b[Pyr]** relative to **1b[Pyr]** is typical for series **2**.

Insertion of a carboxylate group between the cyclohexyl and phenyl ring of **1b[Pyr]** and **2b[Pyr]** induces a SmA phase in **2c[Pyr]**, and widens the mesophase range by over 50 K in **1c[Pyr]** relative to **1b[Pyr]**. Replacement of the carboxylate group in **1c[Pyr]** and **2c[Pyr]** with a CH₂CH₂ linker and substitution of a lateral fluorine atom in **1f[Pyr]** and **2f[Pyr]** decreases the transition temperatures by about 15 K. Substitution of methyl-enebicyclo[2.2.2]octane for cyclohexane in the two anions and removal of the lateral fluorine increases the clearing temperatures in **1g[Pyr]** and **2g[Pyr]** by about 40 K and induces soft crystalline polymorphism in the former. Fig. 5 shows textures of the SmA and an unidentified X phase displayed by **1g[Pyr]**.

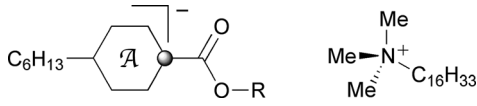

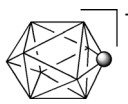
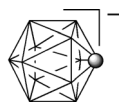
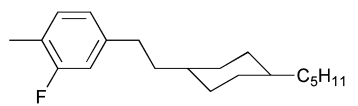
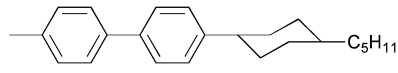
Exchange of the pyridinium cation (**Pyr**) in **1f[Pyr]**, possessing a wide range SmA phase, for cetyltrimethylammonium (**Cetyl**) in **1f[Cetyl]** increases the melting point by about 80 K and loss of mesogenic properties is observed (Table 2). Since compounds in series **2** typically have narrower ranges for mesophases, ion pair

Table 1 Transition temperatures (°C) and enthalpies (kJ mol⁻¹, in parentheses) for **1[Pyr]** and **2[Pyr]**^d

	R	1 , $\bar{A} =$	2 , $\bar{A} =$
a		Cr ₁ 64 Cr ₂ 101 Cr ₃ 107 I (9.2) (3.4) (15.1) ^b	Cr 117 I (27.4)
b		Cr 128 (X' 129) ^c X 153 SmA 163 I (19.3) (3.2) (2.4) (4.5) ^b	Cr ₁ 162 Cr ₂ 178 I (9.8) (24.3)
c		Cr 102 SmA 164 I (43.7) (7.0) ^b	Cr ₁ 109 Cr ₂ 119 SmA 161 I (7.7) (14.9) (6.2)
d		Cr 131 [SmA 98 N 110] I ^d (45.4)	Cr 155 [SmA 97 N 122] I ^d (46.9)
e		Cr ₁ 32 Cr ₂ 123 SmA 132 N 137 I (9.8) (43.2) (0.6) (1.3)	Cr134 (SmA 133) ^c N 144 I (43.2) (0.6) (1.3)
f		Cr 87 SmA 148 I (50.1) (10.9)	Cr 99 SmA 146 I (35.7) (8.9)
g		Cr ₁ 123 X' 129 X 132 SmA 189 I (41.3) (2.8) (3.3) (11.5)	Cr 150 SmA 182 I (39.2) (13.8)

^a Transition temperatures obtained on heating. ^b Ref. 11 ^c Monotropic transition temperature obtained on cooling. ^d Virtual transition temperatures obtained from binary mixtures with **2e[Pyr]**.

Table 2 Transition temperatures (°C) and enthalpies (kJ mol⁻¹, in parentheses) for selected **Cetyl** ion pairs^a

		
		
	1 , \bar{A} = 	2 , \bar{A} = 
f		Cr ₁ 64 Cr ₂ 169 I (34.4) (54.2)
h		Cr <20 X 184 SmA 229 I (16.9) (7.5)
		b Cr 36 X' 211 X 216 SmA 226 dec (7.6) (1.3) (12.1) (0.8)

^a Transition temperatures obtained on heating. ^b Not prepared.

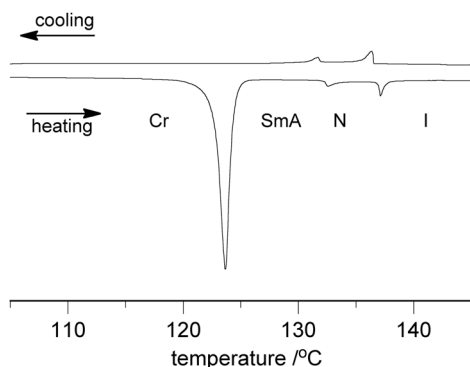


Fig. 3 DSC trace for ion pair **1e[Pyrr]**.

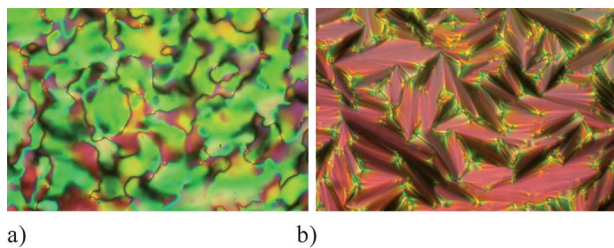


Fig. 4 Optical textures of **1e[Pyrr]** obtained for the same region of the sample upon cooling: (a) nematic phase and (b) SmA phase.

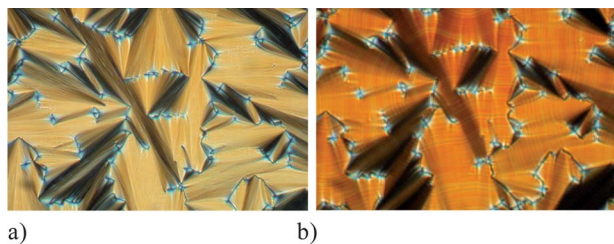


Fig. 5 Optical textures of **1g[Pyrr]** obtained for the same region of the sample upon cooling: (a) SmA phase and (b) unidentified phase X.

2f[Cetyl] was not investigated. In order to induce mesogenic behavior in ion pairs with the **Cetyl** cation, the rigid core of anions **1b** and **2b** was extended by addition of a second benzene ring. The resulting ion pairs **1h[Cetyl]** and **2h[Cetyl]** indeed displayed polymorphism with SmA–I transitions near 230 °C. Both ion pairs exhibit a broad range (>160 K) soft crystalline phase.

A detailed analysis of the two series of compounds demonstrates that the SmA phase is generally less thermodynamically stable in the 12-vertex derivatives by up to 6 K than in the 10-vertex analogues, while the nematic phase appears to be more stable in the 12-vertex compounds. Interestingly, these observations for series **1** and **2** are opposite to results found in non-ionic LC containing the carborane analogues of monocarborates **A** and **B**.^{24,25}

Binary mixtures

Virtual transition temperatures for the two non-mesogenic azo derivatives **1d[Pyrr]** and **2d[Pyrr]** were extrapolated from transition temperatures obtained for low concentration solutions in **2e[Pyrr]**. For both additives the phase transition temperatures changed approximately linearly with respect to the composition of the mixture, as shown for **2d[Pyrr]** in **2e[Pyrr]** in Fig. 6, which demonstrates ideal miscibility of the components. Crystallization of the components was significantly suppressed in the mixture. The SmA–N transition was found to be monotropic for all mixtures and the host, and temperatures for both transitions, N–I and SmA–N, were recorded on cooling. The least square fitting lines had high correlation factor ($r^2 > 0.992$) and the extrapolated temperatures (Table 1) have uncertainty of ± 1 K.

10 mol% solutions of **1f[Pyrr]** in non-ionic esters **8**²⁶ and **9**²⁷ were investigated briefly. The mixture of **1f[Pyrr]** and **8** appears to be completely homogenous, and its SmA–I transition temperature of 175 °C is essentially the same as the pure host. A similar solution in ester **9** was homogenous in the isotropic phase, however, upon cooling the SmA phase separated from the nematic.

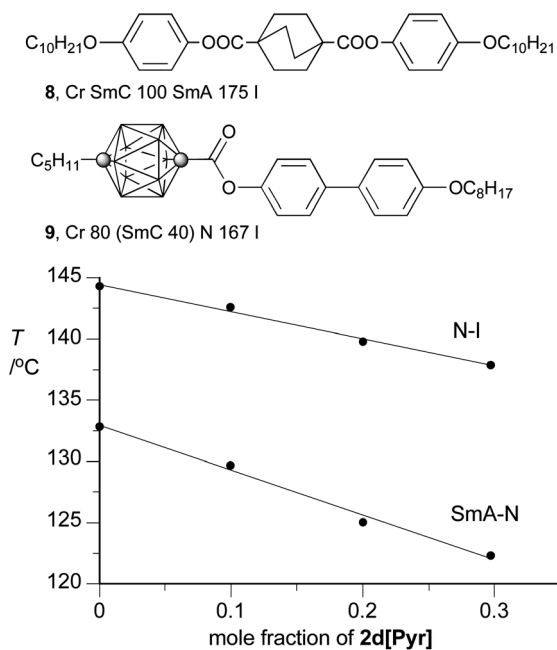


Fig. 6 A plot of N-I and SmA-N transition temperatures for binary mixtures of **2d**[Pyr] in **2e**[Pyr] as a function of mole fraction of **2d**[Pyr].

Powder X-ray diffraction

Esters **1e**[Pyr]–**1g**[Pyr], **2f**[Pyr], and **2g**[Pyr] were investigated by X-ray powder diffraction. Data was collected on cooling from the isotropic phase, and XRD results are shown in Table 3, Fig. 7 and Fig. 8.

The XRD results confirmed the presence of SmA phase in all five compounds. The diffractograms of the SmA phase consist of a series of sharp, commensurate reflections in the small angle region, corresponding to smectic layer periodicity, and a broad halo centered at about 5 Å in the wide-angle region (Fig. 7). The halo is attributed to the average alkyl chain-alkyl chain correlation distance and to the correlations involving larger structural units such as the boron clusters. The SmA layer thickness d , indicated by the d_{001} reflection, is about 26 Å for all five samples. A comparison with calculated molecular lengths (HF/6-31G(d)), demonstrates that the degree of interdigitation in the SmA is about 0.2 in all five compounds (Table 3).

Temperature-dependent XRD analysis demonstrated that the layer thickness d contracts in the SmA phase with increasing temperature for esters **1e**[Pyr], **1f**[Pyr], **2f**[Pyr] and **2g**[Pyr] for

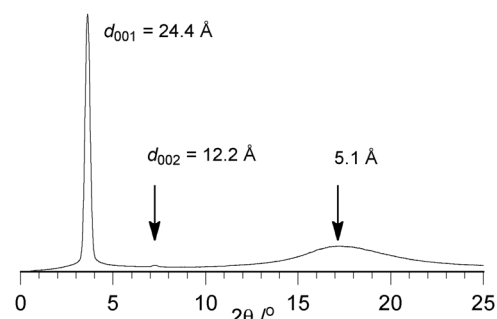


Fig. 7 X-ray diffraction pattern for **2f**[Pyr] in SmA phase at 136 °C.

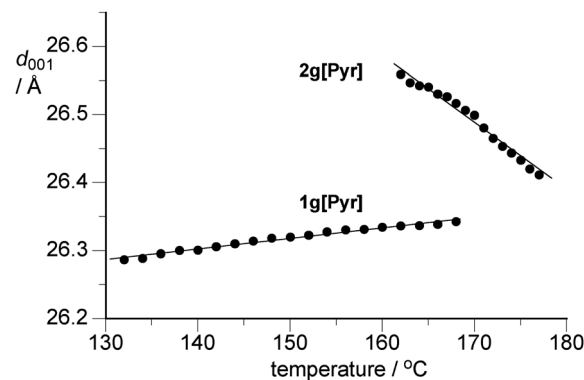


Fig. 8 Layer thickness d in SmA phase as a function of temperature for ion pairs **1g**[Pyr] and **2g**[Pyr].

which the thermal expansion coefficient κ ranges from +0.16 to -3.38 pm K^{-1} (Table 3). Interestingly, ester **1g**[Pyr] undergoes layer expansion upon heating with thermal expansion coefficient of $+0.16 \text{ pm K}^{-1}$ (Fig. 8), while the smectic layer in its *{closo-CB₁₁}* analogue, **2g**[Pyr], relatively quickly contracts with increasing temperature ($\kappa = -1.02 \text{ pm K}^{-1}$). In contrast, in the pair **1f**[Pyr] and **2f**[Pyr] thermal expansion coefficients κ are similar and small.

Summary and conclusions

The results demonstrate that the *[closo-1-CB₁₁H₁₂]⁻* anion (**B**) is an effective structural element of ionic liquid crystals such as **2**, and that their preparation is more efficient than the analogous derivatives of the *[closo-1-CB₉H₁₀]⁻* anion, **1**. In general, ion pairs that have a total of 4 rigid structural elements (rings and the

Table 3 The molecular interdigitation in selected compounds and phases

Compound	Length $L^a/\text{\AA}$	Temperature $T/^\circ\text{C}$	Phase	Cell constant $c^b/\text{\AA}$	$\kappa^c/\text{pm K}^{-1}$	Interdigitation $I = (L - c)/L$
1e [Pyr]	34.0	125	SmA	27.8	-3.38	0.18
1f [Pyr]	31.8	130	SmA	24.5	-0.25	0.23
1g [Pyr]	32.7	150	SmA	26.3	+0.16	0.20
		126	X	26.6		0.19
		116	X'	26.8		0.18
2f [Pyr]	31.8	120	SmA	24.4	-0.17	0.23
2g [Pyr]	32.4	165	SmA	26.5	-1.02	0.18

^a Most extended molecular conformation optimized at the HF/6-31G(d) level of theory. ^b Calculated from d_{001} . ^c Thermal expansion coefficient.

monocarbaborate cage) exhibit liquid crystalline properties. This includes pyridinium salts of three ring anions (e.g. **1b**[Pyr] and **2f**[Pyr]), and cetyltrimethylammonium salts of four-ring anions (**1h**[Cetyl] and **2h**[Cetyl]). None of the ion pairs containing 3 rigid structural elements (e.g. **1a**[Pyr] and **1h**[Cetyl]) form mesophases. All mesogenic ion pairs exhibit a SmA phase. Temperature-dependent XRD analysis of 5 mesogens showed partial interdigitation (~20%). Thermal expansion coefficient κ of the SmA phase was found to be negative for four of the mesogens and positive for ion pair **1g**[Pyr]. In addition to the SmA phase, azo derivatives **1d**[Pyr], **2d**[Pyr], **1e**[Pyr] and **2e**[Pyr] exhibit a nematic phase, that is rarely observed in ILC. The nematic phase is more stable for the {*closo*-CB₁₁} derivatives than for 10-vertex analogues, while the {*closo*-CB₉} derivatives exhibit a somewhat greater stability of the SmA phase.

Binary mixture studies demonstrated ideal miscibility of structurally similar ion pairs **1d**[Pyr] and **2d**[Pyr] in **2e**[Pyr], and a homogenous 10 mol% solution of **1f**[Pyr] in a non-ionic smectogen. These results are important in the context of developing ambient temperature Li⁺ cation conducting materials. Also in this context, the preparation of a Cs⁺ salt, **1h**[Cs], has been demonstrated, although this material is not mesogenic and has high melting point.

Further studies will concentrate on modification of the flexible chain to incorporate functional groups chelating the metal ion, and to study metal salts in the context of electrolytes for battery applications.

Experimental part

¹H NMR spectra were obtained at 400 MHz in acetone-*d*₆ (δ 2.04 ppm) or CDCl₃ (δ 7.26 ppm). ¹¹B NMR spectra were recorded at 128 MHz. Chemical shifts were referenced to the solvent (¹H) or to an external sample of B(OH)₃ in MeOH (¹¹B, δ = 18.1 ppm). The preparation and characterization details of *N*-butyl-4-heptyloxy pyridinium bromide (**[Pyr]Br**),¹¹ phenols **5a**,²⁸ **5b**,²⁹ **5c**,³⁰ **5d**,³¹ **5e**,³² and **5h**,³³ and also ion pairs **1a**[Pyr]–**1c**[Pyr]¹¹ were reported previously.

Optical microscopy was performed using a PZO Biolar microscope equipped with an HCS402 Instec hot stage. Thermal analysis was obtained using a TA Instruments 2920 DSC. Transition temperatures (onset) and enthalpies were obtained using small samples (~0.5 mg) and a typical heating/cooling rate of 5 K min⁻¹ under a flow of nitrogen gas. XRD measurements were carried out on unoriented and uncovered samples placed on a temperature-controlled glass plate using GADDS X-ray diffractometer (Cu-K α , λ = 1.5405 Å). XRD patterns were collected in the range of 1.5°–35° on cooling. Layer spacing (cell constant *c*) was determined from the (001) reflection.

Preparation of binary mixtures

Binary mixtures were prepared by dissolving both components in small amounts of dry MeCN, subsequent evaporation of the solvent, and drying the resulting homogenous material at 130 °C for several hours. The hot homogenous mixture was transferred to an aluminum pan and analyzed by DSC. Transition temperatures of the mixtures were taken as peak temperature on the second cooling cycle.

General procedure for preparation of esters **1** and **2**

Phenol **5** (1.5 equivalents) was added to a colorless solution of acid [*closo*-1-CB₉H₈-1-COOH-10-C₆H₁₃]⁻[NMe₄]⁺ (**3**[NMe₄]) or [*closo*-1-CB₁₁H₁₀-1-COOH-12-C₆H₁₃]⁻[NEt₄]⁺ (**4**[NEt₄]), DCC (1.0 equivalent), and DMAP (0.1 equivalents) in anhydrous CH₂Cl₂. The reaction mixture was stirred overnight at rt, and the reaction progress was monitored by TLC (*R*_f 0.5, CH₃CN/CH₂Cl₂, 1 : 9). The solvent was removed *in vacuo*, and the crude product was isolated by column chromatography (SiO₂, CH₃CN/CH₂Cl₂, 1 : 9). The resulting ion pair, **1**[NMe₄] or **2**[NEt₄], was washed with hot hexane and used in the subsequent step for cation exchange without further purification. Typical yields for this procedure were above 80%.

N-Butyl-4-heptyloxy pyridinium bromide (**[Pyr]Br**, 1.0 equivalent) or cetyltrimethylammonium bromide (**[Cetyl]Br**, 1.0 equivalent) were added to a solution of ester **1**[NMe₄] or **2**[NEt₄] in CH₂Cl₂. Water was added, and the biphasic system was stirred vigorously until all the precipitate had dissolved. The CH₂Cl₂ layer was separated, and the aqueous layer was extracted with additional CH₂Cl₂. The CH₂Cl₂ layers were combined, washed with H₂O, dried (Na₂SO₄), and evaporated giving **1**[Pyr], **2**[Pyr], **1**[Cetyl] or **2**[Cetyl] as crystalline solids, which were further purified by recrystallization from aqueous alcohol. Some pyridinium salts were purified further by column chromatography (CH₃CN/CH₂Cl₂, 1 : 9) and then by repeated recrystallization from aqueous alcohol. The resulting crystals were dried in vacuum at ambient temperature. Typical yields of the final ion pairs range from 20%–40% based on the starting acid **3**[NMe₄] or **4**[NEt₄]. Analytical data for ion pairs is provided in ESI.†

Acknowledgements

Financial support for this work was received from the National Science Foundation (DMR-0907542). BR thanks the Vanderbilt University Graduate School for a Dissertation Enhancement Grant that permitted him to conduct the XRD measurements at the University of Warsaw. We thank Mr. Jacek Pecyna and Mr. Richard P. Denicola for assistance with the synthesis of **6**[NEt₄], and Prof. Roman Dabrowski of MUT, Warsaw, Poland for the gift of phenols **5f** and **5g**.

References

- 1 K. V. Axenov and S. Laschat, *Materials*, 2011, **4**, 206–259.
- 2 K. Binnemans, *Chem. Rev.*, 2005, **105**, 4148–4204.
- 3 M. Yoshio, T. Mukai, K. Kanie, M. Yoshizawa, H. Ohno and T. Kato, *Adv. Mater.*, 2002, **14**, 351–354; M. Yoshio, T. Mukai, H. Ohno and T. Kato, *J. Am. Chem. Soc.*, 2004, **126**, 994–995; M. Yoshio, T. Kagata, K. Hoshino, T. Mukai, H. Ohno and T. Kato, *J. Am. Chem. Soc.*, 2006, **128**, 5570–5577.
- 4 T. Ichikawa, M. Yoshio, A. Hamasaki, T. Mukai, H. Ohno and T. Kato, *J. Am. Chem. Soc.*, 2007, **129**, 10662–10663.
- 5 S. Yazaki, Y. Kamikawa, M. Yoshio, A. Hamasaki, T. Mukai, H. Ohno and T. Kato, *Chem. Lett.*, 2008, **37**, 538–539.
- 6 Y. Grabovskiy, A. Kovalchuk, A. Grydyakina, S. Bugaychuk, T. Mirnaya and G. Klimusheva, *Liq. Cryst.*, 2007, **34**, 599–603.
- 7 H. Shimura, M. Yoshio, K. Hoshino, T. Mukai, H. Ohno and T. Kato, *J. Am. Chem. Soc.*, 2008, **130**, 1759–1765.
- 8 Y. Abu-Lebdeh, A. Abouimrane, P.-J. Alarco and M. Armand, *J. Power Sources*, 2006, **154**, 255–261.
- 9 N. Yamanaka, R. Kawano, W. Kubo, T. Kitamura, Y. Wada, M. Watanabe and S. Yanagida, *Chem. Commun.*, 2005, 740–742;

- R. Kawano, M. K. Nazeeruddin, A. Sato, M. Grätzel and M. Watanabe, *Electrochem. Commun.*, 2007, **9**, 1134–1138.
- 10 C. A. Reed, *Acc. Chem. Res.*, 1998, **31**, 133–139; S. H. Strauss, *Chem. Rev.*, 1993, **93**, 927–942; I. Krossing and I. Raabe, *Angew. Chem., Int. Ed.*, 2004, **43**, 2066–2090.
- 11 B. Ringstrand, H. Monobe and P. Kaszynski, *J. Mater. Chem.*, 2009, **19**, 4805–4812.
- 12 B. Neises and W. Steglich, *Angew. Chem., Int. Ed. Engl.*, 1978, **17**, 522–524.
- 13 E. Erdik, *Tetrahedron*, 1992, **48**, 9577–9648.
- 14 P. Knochel and R. D. Singer, *Chem. Rev.*, 1993, **93**, 2117–2188.
- 15 B. Grüner, Z. Janousek, B. T. King, J. N. Woodford, C. H. Wang, V. Vsetecka and J. Michl, *J. Am. Chem. Soc.*, 1999, **121**, 3122–3126.
- 16 M. Valášek, J. Štursa, R. Pohl and J. Michl, *Inorg. Chem.*, 2010, **49**, 10247–10254.
- 17 A. Franken, N. J. Bullen, T. Jelinek, M. Thornton-Pett, S. J. Teat, W. Clegg, J. D. Kennedy and M. J. Hardie, *New J. Chem.*, 2004, **28**, 1499–1505.
- 18 J. Pecyna, R. P. Denicola, B. Ringstrand, A. Jankowiak and P. Kaszynski, *Polyhedron*, 2011, **30**, 2505–2513.
- 19 D. Demus; L. Richter. *Textures of Liquid Crystals*; 2nd ed.; VEB: Leipzig, 1980; G. W. Gray; J. W. G. Goodby. *Smectic Liquid Crystals-Textures and Structures*; Leonard Hill: Philadelphia, 1984; I. Dierking. *Textures of Liquid Crystals*; Wiley-VCH: Weinheim, 2003.
- 20 J. Baudoux, P. Judeinstein, D. Cahard and J.-C. Plaquevent, *Tetrahedron Lett.*, 2005, **46**, 1137–1140; K. Goossens, P. Nockemann, K. Driesen, B. Goderis, C. Görrler-Walrand, K. Van Hecke, L. Van Meervelt, E. Pouzet, K. Binnemans and T. Cardinaels, *Chem. Mater.*, 2008, **20**, 157–168; W. Li, J. Zhang, B. Li, M. Zhang and L. Wu, *Chem. Commun.*, 2009, 5269–5271; X. Cheng, X. Bai, S. Jing, H. Ebert, M. Prehm and C. Tschierske, *Chem.–Eur. J.*, 2010, **16**, 4588–4601; X. Liu, J.-L. Liu, B. Cai and X.-M. Ren, *Inorg. Chem. Commun.*, 2011, **14**, 1428–1431.
- 21 D. W. Bruce, D. A. Dunmur, P. M. Maitlis, P. Styring, M. A. Esteruelas, L. A. Oro, M. B. Ros, J.-L. Serrano and E. Sola, *Chem. Mater.*, 1989, **1**, 479–481; Y. G. Galyametdinov, A. A. Knyazev, V. I. Dzhabarov, T. Cardinaels, K. Driesen, C. Görrler-Walrand and K. Binnemans, *Adv. Mater.*, 2008, **20**, 252–257.
- 22 M. T. McCaffrey and J. A. Castellano, *Mol. Cryst. Liq. Cryst.*, 1972, **18**, 209–225.
- 23 R. Stainsträsser and L. Pohl, *Z. Naturforsch.*, 1971, **26b**, 577–580.
- 24 A. Januszko, P. Kaszynski, M. D. Wand, K. M. More, S. Pakhomov and M. O'Neill, *J. Mater. Chem.*, 2004, **14**, 1544–1553.
- 25 A. Januszko, K. L. Glab, P. Kaszynski, K. Patel, R. A. Lewis, G. H. Mehl and M. D. Wand, *J. Mater. Chem.*, 2006, **16**, 3183–3192.
- 26 P. Kaszynski, A. Januszko, K. Ohta, T. Nagamine, P. Potaczek, V. G. Young, Jr and Y. Endo, *Liq. Cryst.*, 2008, **35**, 1169–1190.
- 27 A. G. Douglass, K. Czuprynski, M. Mierzwa and P. Kaszynski, *Chem. Mater.*, 1998, **10**, 2399–2402.
- 28 M. E. Neubert, P. J. Wildman, M. J. Zawaski, C. A. Hanlon, T. L. Benyo and A. De Vries, *Mol. Cryst. Liq. Cryst.*, 1987, **145**, 111–158.
- 29 K. Ohta, A. Januszko, P. Kaszynski, T. Nagamine, G. Sasnouski and Y. Endo, *Liq. Cryst.*, 2004, **31**, 671–682.
- 30 A. Januszko and P. Kaszynski, *Liq. Cryst.*, 2008, **35**, 705–710.
- 31 J. M. Kuiper, R. Hulst and J. B. F. N. Engberts, *Synthesis*, 2003, 695–698.
- 32 F. Vicentini, M. Mauzac, R. Laversanne, P. Pochat and J. P. Parneix, *Liq. Cryst.*, 1994, **16**, 721–733.
- 33 B. Ringstrand, J. Vroman, D. Jensen, A. Januszko, P. Kaszynski, J. Dziaduszek and W. Drzewinski, *Liq. Cryst.*, 2005, **32**, 1061–1070.